

# Laser Beam Shaping with Membrane Deformable Mirrors

Brian G Henderson<sup>1</sup> and Justin D. Mansell

Active Optical Systems, LLC, 2021 Girard Ste 150, Albuquerque, NM 87106

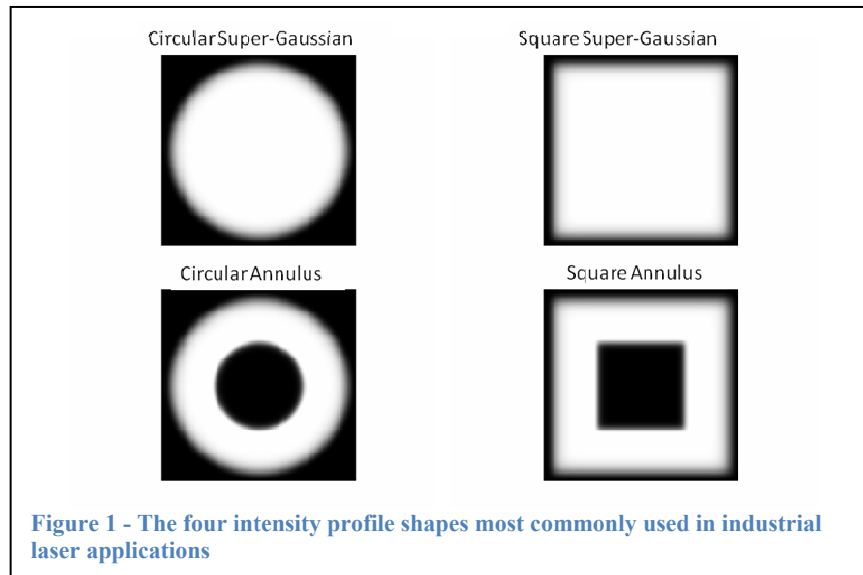
## ABSTRACT

The performance of laser machining systems can often be improved by adjusting the intensity profile of the beam on the target. Shaping a laser intensity profile can be efficiently accomplished by adjusting the spatial phase of the beam before propagating the beam a distance to the target. Beam shaping can be accomplished with passive diffractive elements, but this technique is only capable of creating a single intensity profile and is usually very sensitive to the input beam characteristics. Beam shaping with active optical elements like deformable mirrors can enable the system to achieve multiple shapes and compensate for non-ideal input beams, but can be very expensive. We present here a demonstration of laser beam shaping with low-cost membrane deformable mirrors.

Keywords: Laser Beam Shaping, Adaptive Optics, Membrane Deformable Mirror

## 1. INTRODUCTION

Beam shaping has been explored for many years for industrial and research applications like laser materials processing and photolithography. The intensity profile of a laser beam can be shaped with either amplitude or phase modulation of the beam. Amplitude modulation is effective, but typically wastes a significant amount of the laser energy. When properly performed, phase modulation of a beam can remap the intensity in a way that is virtually lossless, thus making it much more efficient for commercial use.



In this effort, we will focus on shaping a Gaussian beam into four shapes that are generally applicable to industrial applications: elliptical super-Gaussian (or top-hat), rectangular super-Gaussian, elliptical annulus, and rectangular annulus. Figure 1 shows these four intensity profiles.

The shaping will be accomplished using an Active Optical System (AOS) metric adaptive optics (AO) system [2]. The system consists of a polymer membrane deformable mirror, USB interface drive

<sup>1</sup> [bhenderson@mza.com](mailto:bhenderson@mza.com); phone 1 505 245-9970 x160

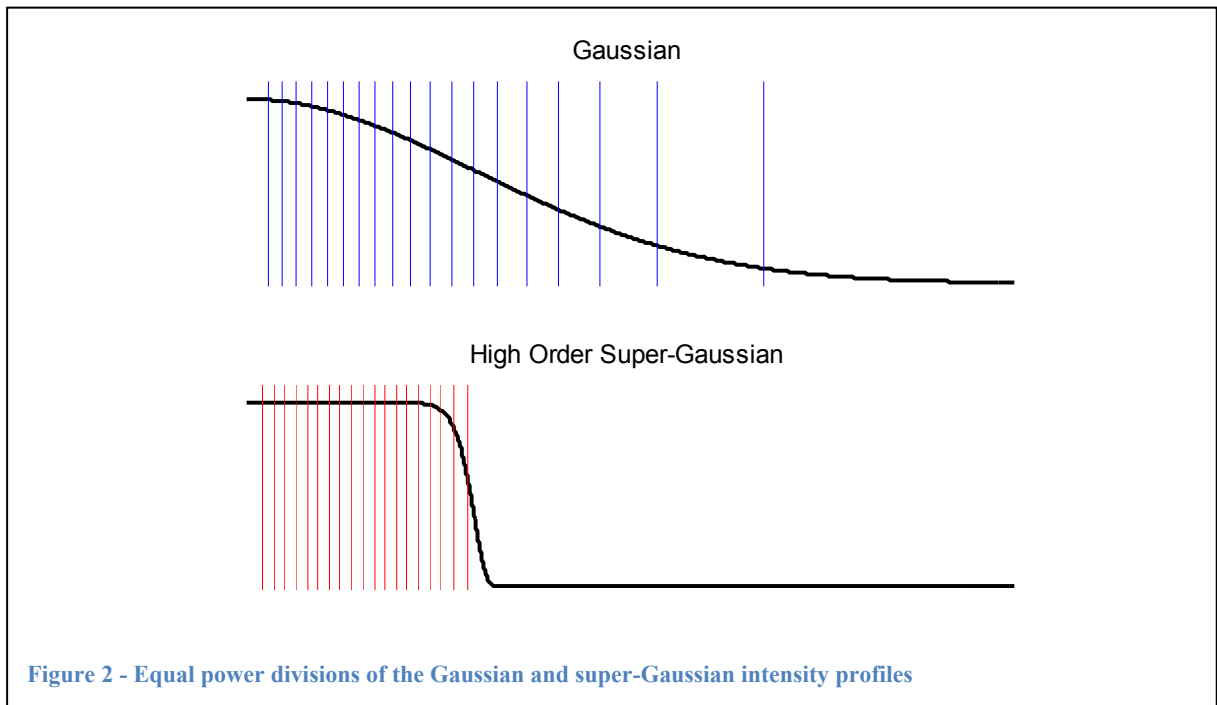
electronics, a high speed 1394 CMOS camera for feedback, and metric AO software. By using a metric AO approach instead of fixed optics to shape the beam, the system is able to compensate aberrations in the system and is resistant to non-ideal (non Gaussian) input beams and misalignments.

## 2. BACKGROUND

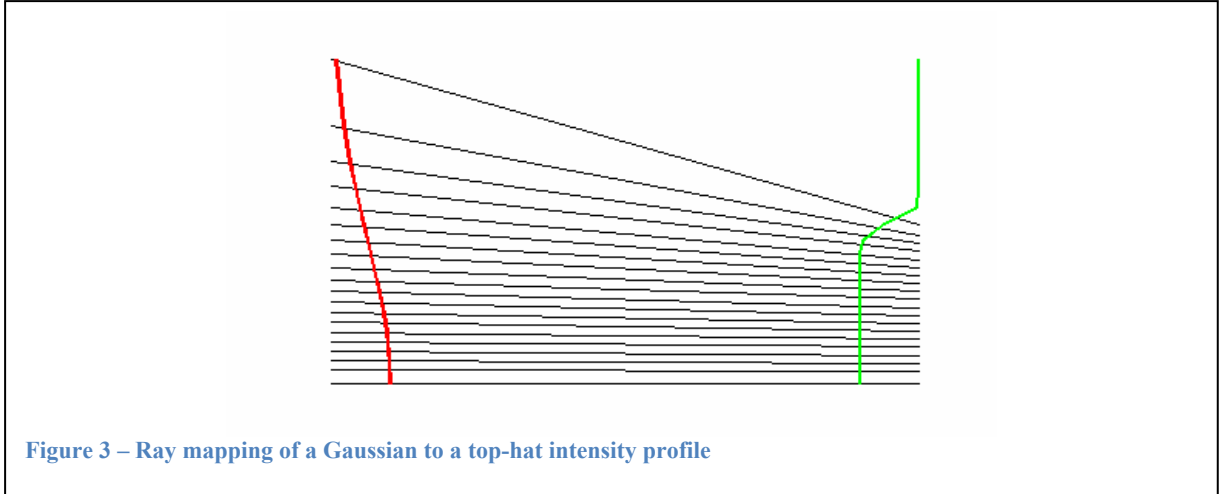
The theory for beam shaping has been outlined in detail in Dickey's book Laser Beam Shaping [1], but one instructive technique, ray mapping, will be summarized here. Ray mapping involves dividing up the beam into equal energy sections and adjusting the phase tilt of the input beam to move the energy from one section to another. This technique is the most intuitive and useful for education purposes. To illustrate this technique, we will show how a Gaussian intensity profile can be converted into a super-Gaussian intensity profile. The super-Gaussian profile is given by

$$\exp\left(-\left(\frac{r}{w}\right)^N\right)$$

where  $r$  is the radius,  $w$  is the radial size of the super-Gaussian, and  $N$  is the order of the super-Gaussian.

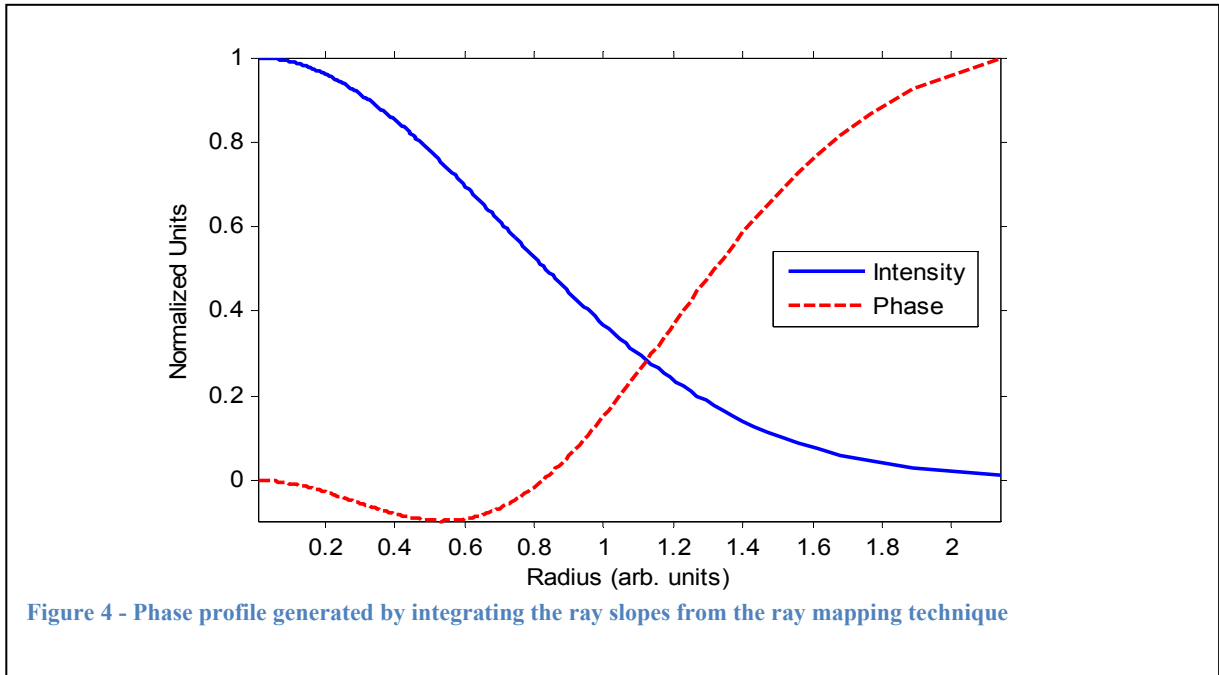


We will work with symmetric radial profiles here for convenience, but this analysis can be extended to more general cases. The first step is to generate each profile and normalize the power by dividing by the integrated intensity. Then we divide each of the profiles into equal intensity sections. Figure 2 shows the equal power divisions of the Gaussian and top-hat radial profiles. For ray-mapping, each of these equal power sections is then mapped to a corresponding section in the output profile starting at the central location. Figure 3 shows how the rays map between the two intensity profiles.



Once the ray mappings have been established, they form a set of slopes that can be integrated to create a desired phase profile. If the beams are significantly different in size, the resulting phase profile has a large amount of focus, which, in the lab, can be accomplished with an external lens. To better illustrate the phase profile, we generated the Gaussian to top-hat profile using profiles of almost the same size.

Figure 4 shows the result of integrating the ray slopes to create a phase profile required to generate a super-Gaussian intensity profile from a Gaussian beam. The profile can be divided into converging and diverging sections. The center portion is diverging since the curvature is facing down. This curvature causes the concentration of energy in the center section of the Gaussian beam to spread out. In the next section, starting at  $r \approx 0.4$ , the phase front causes the light to converge toward the center of the beam, thereby concentrating the light. The combination of these two effects (spreading out the center and concentrating the edge) creates a super-Gaussian intensity profile after propagating a distance from the application of the phase profile.



The phase profile required to create the other three objective shapes are similar to this one. From even this basic simulation, we can see that the phase profile required to map a Gaussian into a super-Gaussian is actually a very low-order distortion that can be easily created with the smooth continuous surface of a membrane deformable mirror.

### 3. APPROACH

While useful for developing intuition, the ray mapping technique assumes the incoming beam is known and un-aberated. For real-world systems, this usually is not the case. For shaping real-world laser beams, an approach is desired that does not make any assumptions about the shape of the incoming beam. By using a global optimization algorithm to control the deformable mirror (metric AO), useful output shapes can be obtained even from aberated input beams.

#### 3.1. Shape Definition

In order to support all of the desired beam shapes, the computation of the desired shape,  $D$ , was performed in two steps: inner shape definition and outer shape definition. To obtain the final shape, the inner shape is subtracted from the outer shape. This arrangement allows annular patterns to be formed. Rectangular and elliptical combinations of outer and inner shapes are supported. A user interface for configuring desired beam shapes is included in the AOS metric AO software. Given an inner and outer shape, the following equation is used to compute the final desired shape:

$$D(x, y) = S_o(x, y) - S_i(x, y)$$

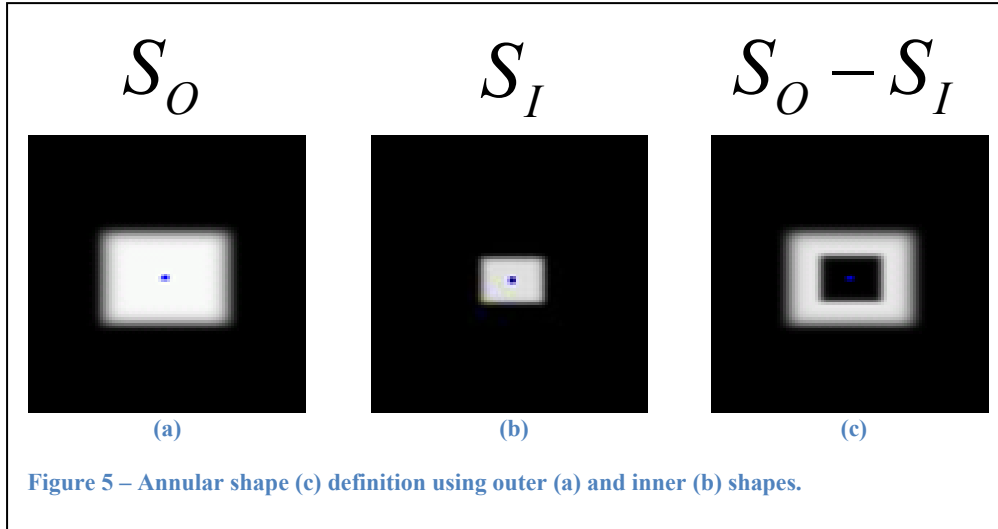
where  $S_o$  is the outer shape and  $S_i$  is the inner shape. Figure 5 shows the inner and outer shapes for a rectangular annular super-Gaussian. The blue squares in the center of the figures correspond to the first moment of the shape. The inner and outer shapes can be either a rectangular super-Gaussian or elliptical super-Gaussian. The following equations may be used to compute rectangular and elliptical super-Gaussians:

$$S_{elliptical}(x, y) = A e^{-\left[\left(\frac{x}{x_s}\right)^2 + \left(\frac{y}{y_s}\right)^2\right]^{\frac{n}{2}}} \quad S_{rect}(x, y) = A e^{-\left[\left(\frac{x}{x_s}\right)^{n_x} + \left(\frac{y}{y_s}\right)^{n_y}\right]}$$

where  $A$  is the maximum value,  $n$  is the super-Gaussian order, and  $x_s$  and  $y_s$  are the shape sizes in the x and y directions, respectively. It is also assumed that the origin of the x and y axes is placed at the center of the shape. The coordinates x and y can also be transformed to rotate the entire shape according to the following transformation:

$$\begin{bmatrix} x' \\ y' \end{bmatrix} = \begin{bmatrix} \cos \theta & -\sin \theta \\ \sin \theta & \cos \theta \end{bmatrix} \begin{bmatrix} x \\ y \end{bmatrix}$$

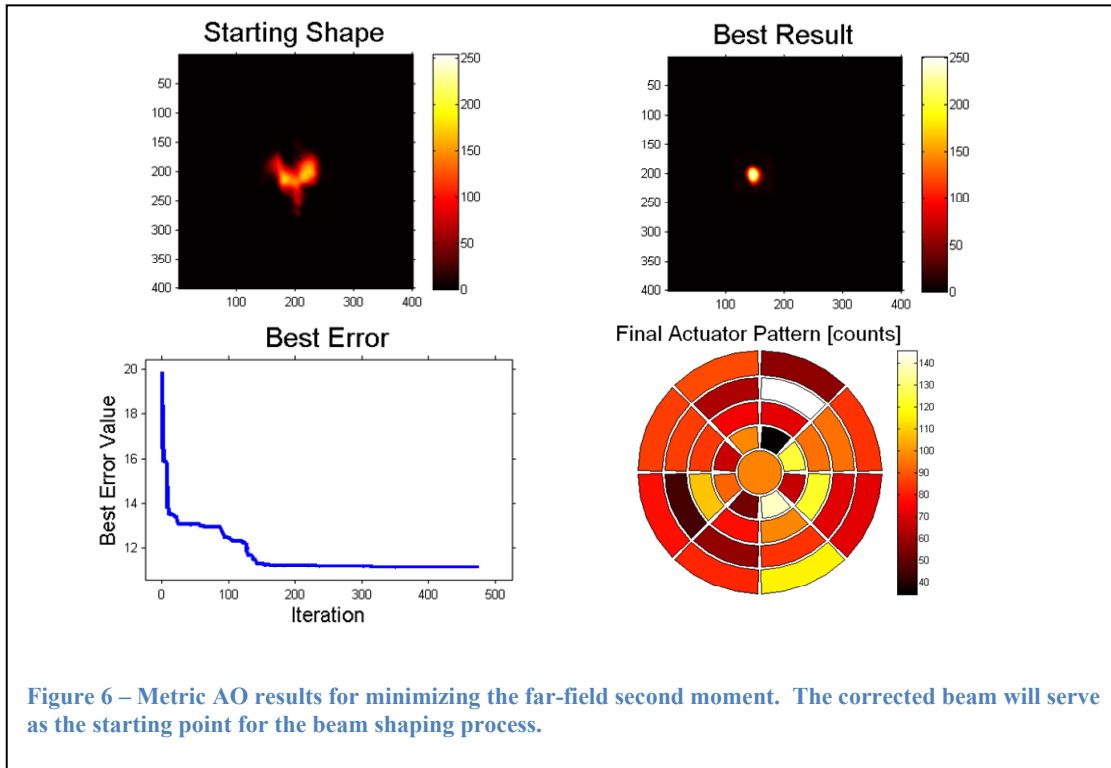
where x-prime and y-prime are the rotated coordinates and theta is the rotation angle.



### 3.2. Experiment Initialization

The starting point of the optimization can have a significant impact on the convergence of the algorithm to the final solution. We found that a spot focused on the sensor plane of the camera provided the greatest probability of success. To achieve a tight focused spot on the camera, we used our metric AO system with the second moment (spot size) of the beam as the merit function.

Figure 6 shows the result of this initialization process. The minimum second moment in this experiment was approximately 6 pixels or 4  $\mu\text{m}$ .



### 3.3. Metric AO for Beam Shaping

In order to address the problems associated with shaping a non-ideal input beam, we chose to use a global optimization algorithm to determine the correct actuator commands to obtain a desired far field beam shape. The optimization algorithm that gave the best shaping results was Guided Evolutionary Simulated Annealing (GESA). GESA is a good choice for many metric AO applications due to its ability to cope with a large number of local minima in the error space. The merit function,  $F$ , is computed by summing the absolute difference between the current far field shape and the desired shape according to the equation

$$F(\vec{c}) = \sum_x \sum_y |M(\vec{c}, x, y) - D(x, y)|$$

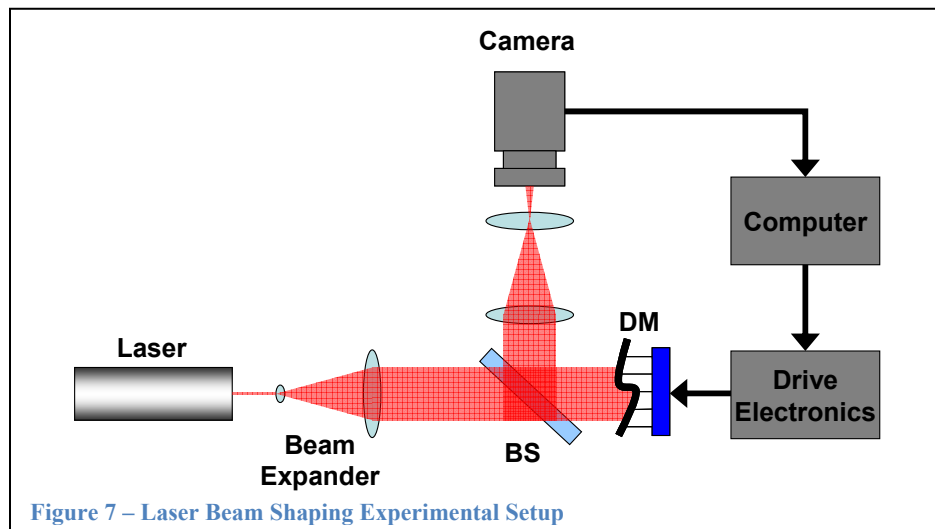
where  $c$  is a vector of commands,  $M$  is the current measured far-field, and  $D$  is the desired far-field shape. Note that the current measured far-field is dependent upon the current set of voltage commands to the DM. We also performed several experiments with a scaled RMS merit function formulation. This particular formulation of the merit function seemed to behave in a very similar manner to the formulation above, but further experiments need to be performed to validate this observation. To remove the effects of global tilt on the beam, the desired far-field shape template,  $D$ , was re-centered over the measured far-field beam at every iteration. Because of this, the beam has a tendency to drift a small amount in the far-field. For most applications, this added tilt can be corrected with a simple tip-tilt mirror, or by placing the DM on a tip-tilt mount.

The algorithm can be summarized as follows:

1. Measure far field shape  $M$
2. Compute far field shape centroid  $C$
3. Center desired shape  $D$  on computed centroid  $C$
4. Compute merit function  $F(c)$
5. Update DM commands according to GESA

## 4. LABORATORY DEMONSTRATION

A laboratory demonstration was conducted in order to validate the modeling results presented in the previous section. The experimental setup consisted of a 633-nm helium-neon laser, AOS polymer membrane deformable mirror, AOS DM drive electronics, 1394 CMOS camera, and various re-imaging optics. A diagram of this setup is shown in Figure 7.



Various beam shapes were attempted including rectangular / elliptical super-Gaussians as well as annular variations on these shapes. The results of the beam shaping process depended heavily on the size and orientation of the shapes chosen. This is due to the optical configuration and configuration of the actuators in the DM.

To generate the following results, the metric AO system was fighting against a couple of factors. First, the optical system had some static aberrations that the DM had to work around. Also, a large intensity profile modulation was introduced into the system by a coverglass over the image sensor in the camera. This manifested itself as a high spatial frequency interference pattern in the far field beam. Future experiments will be performed with the coverglass removed to mitigate this effect. The DM's ability to deal with static aberrations in the optical system is a major advantage of the metric AO beam shaping approach.

The first shape attempted was a simple elliptical super-Gaussian (top-hat) beam. The top-left image in Figure 8 is the desired shape defined in using the AOS metric adaptive optics software. The final result obtained after metric optimization is shown in the top-right image. The fit to the desired shape is quite good, closely matching the peak intensity and lower intensity outer edge of the super-Gaussian shape. The evolution of the best (minimum) error obtained is shown on the bottom-left image. This value is updated each time the optimization algorithm reaches a new optimum. Note the initial rapid convergence to a reasonable solution followed by a slow iterative refinement. This is characteristic of the simulated annealing algorithm used to optimize the shape merit function. The final actuator voltages are visualized in the bottom-right image. The actuator pattern shown is the actual actuator pattern of the deformable mirror used in the metric AO system.

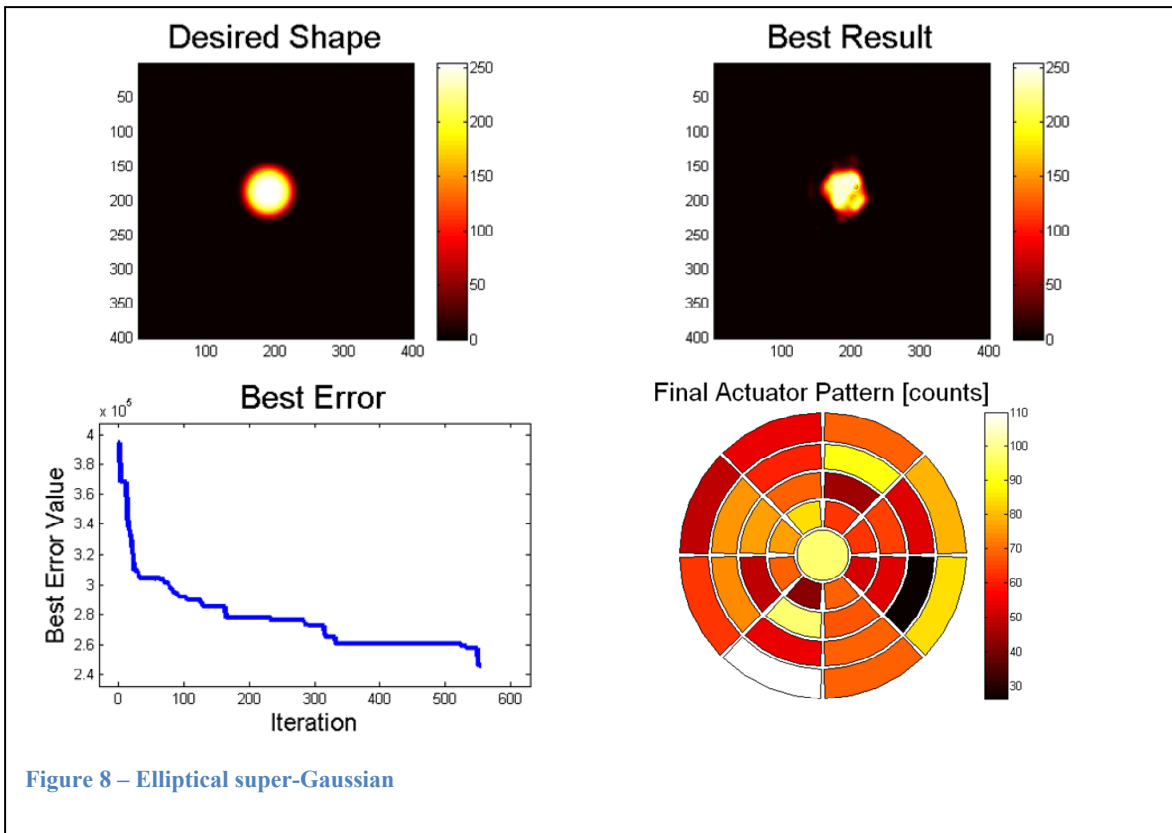


Figure 8 – Elliptical super-Gaussian

Figure 9 shows an elliptical annular super-Gaussian. This shape is characterized by a top-hat beam with a large central obscuration. This shape was considerably more challenging for the AO system. While not

limited by any technical limitation, the AO system had some difficulty redistributing the energy into the area in the bottom of the annulus and removing some of the spurious side-lobes. The energy outside the desired annulus in the side-lobes is probably caused by the poor-quality of the optics in the initial beam expansion telescope causing high spatial frequency terms that are not able to be addressed with the limited DM actuator count. Although the peak intensity between the desired shape and the best result is well matched, the resulting shape only used 70 of the 255 total intensity counts on the camera. From this experiment we learned that dynamic shutter control would be beneficial to beam shaping due to the potential large dynamic range of the results. The extra side-lobes are mostly low intensity and would probably not significantly impact the performance of a laser machining application due to the highly non-linear response of most materials to laser radiation. One other challenge to the system was the coverglass that can clearly be seen making interference fringes from the top-left to the bottom-right of the image.

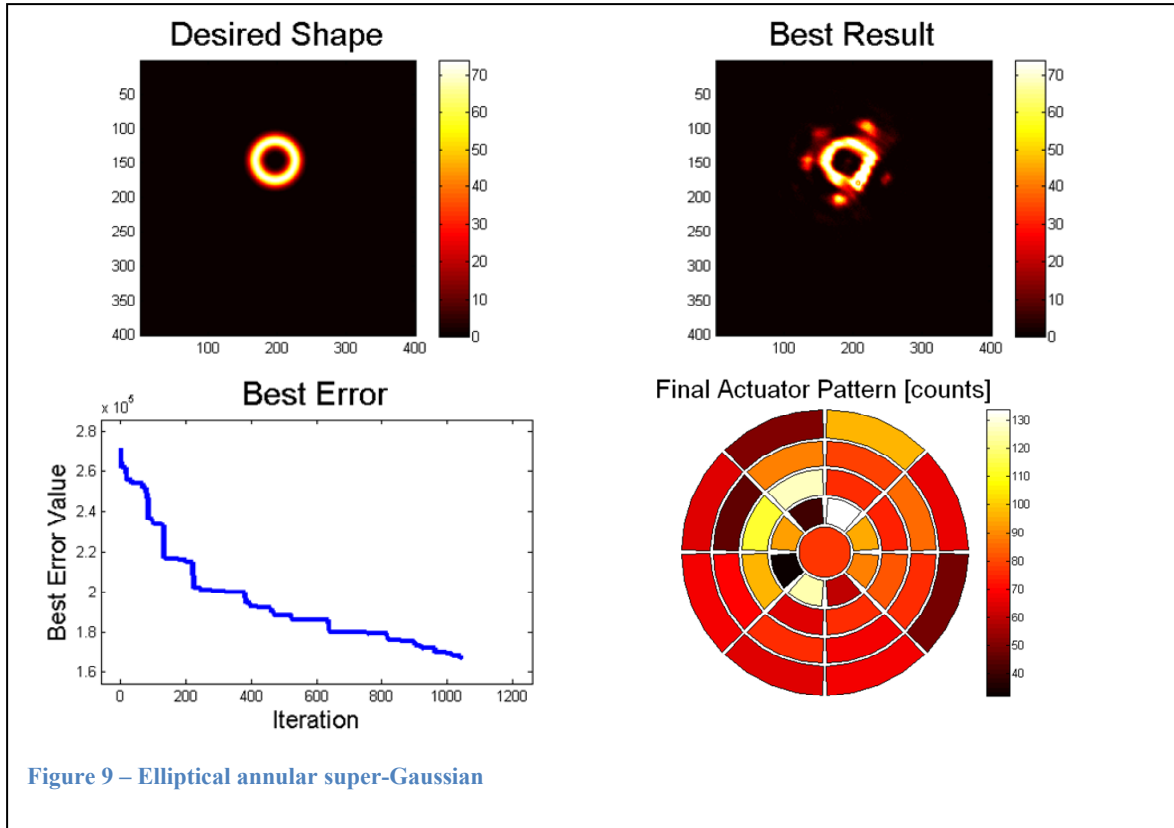


Figure 10 shows an attempt to create a large aspect ratio line focus. The system was quite good at creating various line foci. The best result obtained shows good agreement with the desired shape in many aspects including size, super-Gaussian order (edge sharpness), peak intensity, and flatness of the top of the center of the beam. The desired shape was rotated by 22.5 degrees to take advantage of the DM actuator configuration. Line foci defined to fall centered on radially opposed sets of actuators tended to provide the best results. The effect 22.5 degree rotation can clearly be seen in the resulting actuator values in the bottom-right image of Figure 10.

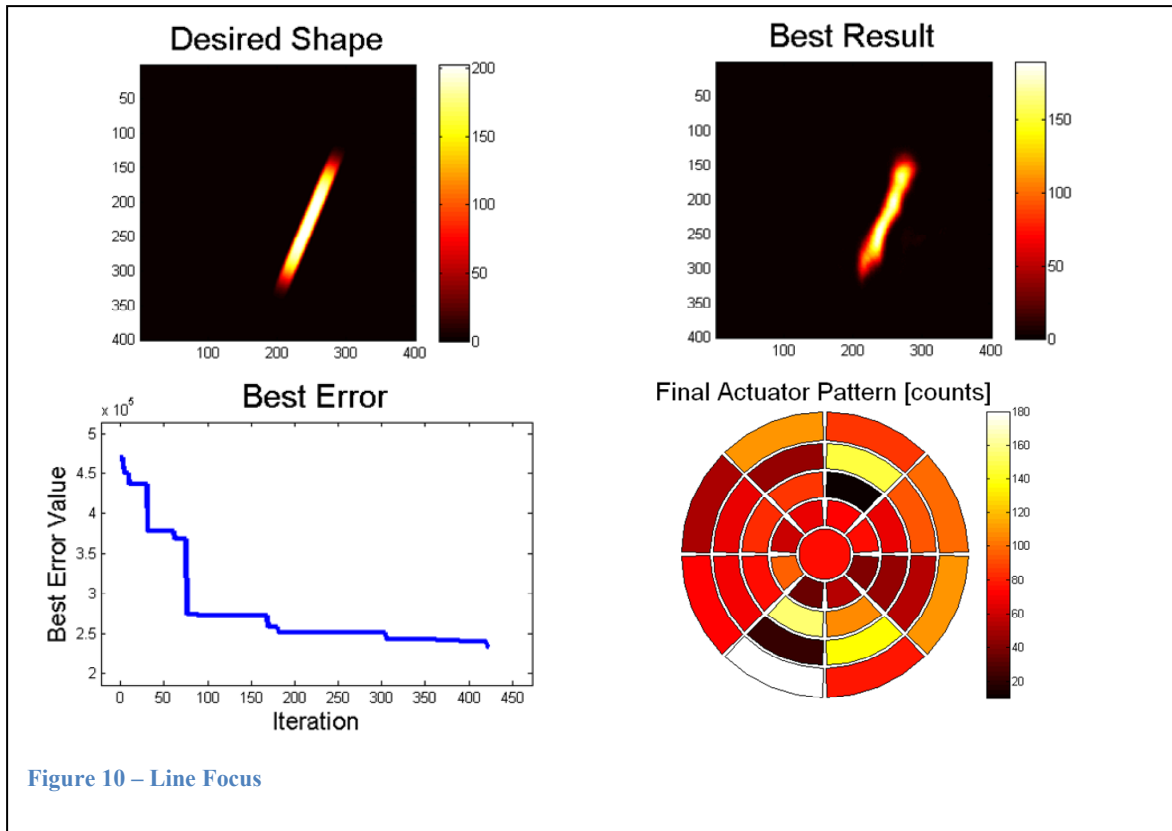


Figure 10 – Line Focus

## 5. CONCLUSIONS AND FUTURE WORK

We demonstrate a simple low-cost adaptive optics system with both the ability to compensate aberrations in the system and perform basic beam shaping based on membrane deformable mirrors. Membrane deformable mirrors offer a unique combination of low-cost, high power (peak and average) handling, and sufficient throw to enable system aberration compensation and beam shaping from the same device. Beam shaping with deformable mirrors has been accomplished in the past, but typically with very high actuator-count deformable mirrors [4]. This beam shaping demonstration showed that a 33-actuator membrane deformable mirror can be used to achieve the beam shapes that are most critical to the industrial users.

The results presented here could be improved with a better optical setup and more advanced algorithms. In our setup, we used a DM with actuators spread out over the entire 25-mm diameter aperture, but the incident Gaussian beam only illuminated approximately the central 15-mm leaving many of the actuators effectively unused. A larger beam would have caused significant clipping at the edges of the beam resulting in power loss and reduced control at the edges. In the future we propose to concentrate our actuators toward the center of the DM to allow higher-resolution control of the phase imposed on the beam. Furthermore, we propose to use a camera without sensor coverglass to avoid artifacts associated with interference between the surfaces of the coverglass.

The metric adaptive optics (MAO) algorithm employed in this effort is effective, but is relatively slow. Once the beam shaping solutions are established they can be applied quickly, but systems with dynamic internal aberrations associated with things like thermal drift or optic heating may require the beam shaping to be frequently repeated, thus reducing the time that the system would be able for work. Furthermore, MAO is not deterministic and can be susceptible to convergence to local minima or, if not configured properly, a lack of convergence at all. As our next steps for this work, we propose to investigate new algorithms that would be higher-speed and allow better performance. One algorithm we have demonstrated in simulation but not in the lab involves leveraging the curvature-device nature of the membrane

deformable mirror coupled with the curvature-nature of the differential equations developed for beam shaping [1]. The shape of a membrane deformable mirror surface,  $z(x,y)$ , with respect to applied spatially-varying voltage,  $V(x,y)$  is given by

$$\nabla^2 z(x,y) = \frac{1}{T} \frac{\varepsilon \cdot A \cdot V(x,y)^2}{2 \cdot d^2}$$

where  $\varepsilon$  is the permittivity of free space,  $A$  is the area of the actuator,  $T$  is a term associated with the tension in the mirror surface, and  $d$  is the distance between the mirror surface and the electrostatic pads. Membrane deformable mirrors are called curvature devices because of the Laplacian nature of this equation. In most situations, the phase profile required for beam shaping is given by

$$\nabla^2 \phi(x,y) = C \frac{I_1(x,y)}{I_2(x,y)}$$

where  $\phi$  is the wavefront phase,  $C$  is a term associated with specific setup of the problem, and  $I_1$  and  $I_2$  are the initial and final spatially-varying intensity profiles normalized for energy conservation[1]. We propose to combine these two equations in analogous fashion to what is done for curvature wavefront control to achieve a fast deterministic method of beam shaping.[3] A simplified equation for the applied spatially-varying voltage to the DM would be given by

$$V(x,y)^2 = C \frac{I_1(x,y)}{I_2(x,y)} \frac{2 \cdot T \cdot d^2}{\varepsilon \cdot A}$$

To be effective at both beam shaping and system aberration compensation, this result may have to be combined with a separate result to compensate the system aberrations, but may be able to be put inside a control system to achieve a good result without such a combination.

## REFERENCES

- [1] F.M. Dickey and S.C. Holswade, *Laser Beam Shaping: Theory and Techniques*, Marcel Dekker, New York, 2000.
- [2] J.D. Mansell et al., "Low-Cost Compact Metric Adaptive Optics Systems", SPIE Vol. 6711 (2007).
- [3] F. Roddier, "Curvature sensing and compensation: a new concept in adaptive optics," *Appl. Opt.* 27, 1223- 1225 (1988).
- [4] C. C. Beckner and D. W. Oesch, "Implementation of a projection-on-constraints algorithm for beam intensity redistribution", SPIE Vol. 6711 (2007).